

Complex Resistivity Tomography for Environmental Applications

Abelardo Ramirez[#], William Daily[#],
Andrew Binley^{##} & Douglas LaBrecque^{###}

[#]Lawrence Livermore National Laboratory, Livermore, CA 94550, USA

^{##}Lancaster University, Lancaster, LA1 4YQ, UK

^{###}Steamtech, Inc., Bakersfield, CA, USA

Abstract – Complex resistivity may provide valuable information about the structural and hydraulic nature of porous media and fluids contained within those media. The environmental value of such a property is obvious. To date most environmental applications of complex resistivity have focussed on relatively crude data analysis methods and restrictive electrode configurations. New tomographic methods are becoming available that will allow complex resistivity to be employed with arbitrary electrode arrangements. Laboratory trials of our extensions of electrical resistivity tomography to a complex form are reported. The inversion procedure is presented and demonstrated for a range of targets, with resistive and reactive characteristics. The approach is shown to provide useful magnitude and phase images, giving spectral information about the region of interest. The usefulness of imaging resistivity phase is evident when compared with more conventional resistivity tomography, in particular when examined over a range of input frequencies.

Keywords: complex resistivity, inversion, relaxation.

1. INTRODUCTION

Complex resistivity has been widely available for several decades in mineral prospecting industry. With this method resistance data (in terms of magnitude and phase) are collected over a range of input frequencies, typically in the mHz to kHz range, conventionally using electrodes on the ground surface.

Environmental applications of complex resistivity are by no means confined to mineral explorations. There is growing interest in using such information to gain an understanding about the hydraulic properties of the subsurface environment. Clays, for example, will exhibit significant polarisation, which will be reflected in high phase angles. In comparison, sands and gravels will show small phase lags. The intergranular permeability of many rocks will be strongly correlated to pore size distribution, which is closely linked to grain size distribution and thus the spectral response.

It is not just characteristics of the grains within a porous medium that may exhibit characteristic spectra. Observations by [1], [2] and [3] have shown how complex resistivity may give valuable information about contaminants in our groundwaters by examining relaxation curves for porous media contaminated with different

hydrocarbons. Interest is now growing into using complex resistivity for contaminant identification.

We report here on laboratory trials of our extensions of electrical resistivity tomography to a complex form. The inversion procedure is presented and demonstrated for two different targets, with resistive and reactive characteristics.

2. FORWARD PROBLEM

It is assumed that the region of interest may be represented as a two-dimensional complex resistivity distribution $r^*(x,z)$ (* denotes a complex term). If electromagnetic effects can be neglected the forward problem is defined by the Fourier transformed Poisson's equation for a point source with real current I :

$$\frac{\partial}{\partial x} \left(\frac{1}{r^*} \frac{\partial v^*}{\partial x} \right) + \frac{\partial}{\partial z} \left(\frac{1}{r^*} \frac{\partial v^*}{\partial z} \right) - I^2 \frac{v^*}{r^*} = -I d(x) d(z) \quad (1)$$

Here v^* is the transformed complex potential and λ is the transformation variable. This differential equation may be solved using the finite element method for given boundary conditions. Inverse

Fourier transform and appropriate superposition of the calculated potentials yields the complex transfer resistance of an arbitrary electrode configuration in the considered plane, from which a complex resistance can be calculated.

3. INVERSE PROBLEM

Due to the possibly wide range of conductivity it is common to use log transformed parameters within the inversion, that is, $m_j^* = \log_e(\rho_j^*)$ ($j=1,2,\dots,M$), as the parameters of the inversion, where ρ_j^* are the resistivities of one or more elements depending on the parameterisation, M is the number of parameters. Note that the complex logarithm separates real logarithm of magnitude and phase of its argument into real and imaginary parts.

The objective function minimised here consists of the data misfit (with f as the operator of the forward solution) and the model roughness (as used for numerous DC inversion algorithms, see for example [4]):

$$\Phi(\mathbf{m}^*) = [\mathbf{D}^* - f(\mathbf{m}^*)]^T \mathbf{W}^T \mathbf{W} [\mathbf{D}^* - f(\mathbf{m}^*)] + \alpha \mathbf{m}^{*T} \mathbf{R} \mathbf{m}^* \quad (2)$$

The data weighting matrix \mathbf{W} in (2) is composed of the standard deviations of the measurements. \mathbf{R} is a roughness matrix used to force smoothing of the resistivity distribution and stabilise the inverse solution and α is a smoothing parameter.

Minimisation of the linearised objective function in (2) yields the complex linear system of equations

$$(\mathbf{A}^H \mathbf{W}^T \mathbf{W} \mathbf{A} + \alpha \mathbf{R}^T \mathbf{R}) \Delta \mathbf{m}^* = \mathbf{A}^H \mathbf{W}^T [\mathbf{D}^* - f(\mathbf{m}^*)] - \alpha \mathbf{R}^T \mathbf{R} \mathbf{m}^* \quad (3)$$

which is solved for a model perturbation $\Delta \mathbf{m}^*$. In (3) the sensitivity matrix \mathbf{A} is defined as:

$$A_{i,j} = \frac{\partial D_i^*}{\partial m_j^*}$$

The procedure terminates when the desired data misfit has been reached. The method adopted to determine the regularisation parameter α is based on a univariate search at each inverse iteration step. The approach is similar to that originally employed by [5].

The linear system of equations in (3) is solved using the conjugate gradient (CG) method, which is developed for complex systems in, for example, [6]. For preconditioning a simple diagonal scaling of the matrix is used.

4. APPLICATION TO A SCALED MODEL

4.1 Experimental setup

To demonstrate the approach a scale model was designed as follows. Two lines of 10 equally spaced electrodes were aligned in parallel, 20cm apart. The electrodes were secured to a plastic frame and placed on the water surface in a 3.1m diameter, 2.45m deep fibreglass water tank. This arrangement was adopted as a scale model of a typical cross borehole electrode arrangement (the water tank acting as an 'infinite' domain. The resistivity of the water within the tank was 32 ohm.

Two targets were prepared, a PVC tube, 6.7cm in diameter and the same tube with copper tape secured along the length of the tube. Each target was placed with its long axis perpendicular to the plane of the 'cross-borehole' arrangement of electrodes. Figure 1 shows the arrangement used.

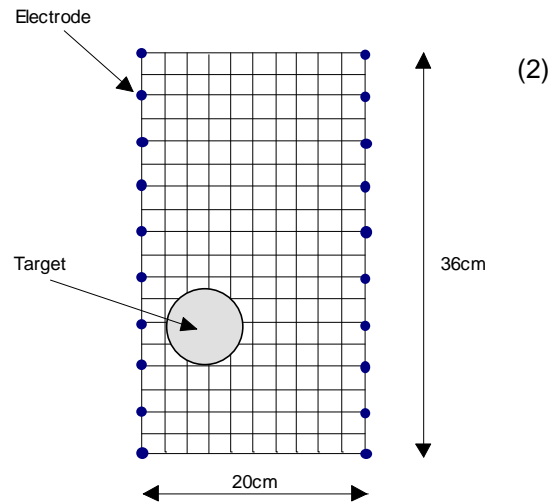


Figure 1: Experimental layout

Complex resistance data were collected for both target types. Each measurement is the resistance measured between two electrodes with current injected at two other electrodes. Each data set consists of 340 measurements, half of which were reciprocal measurements (current and potential electrodes switched) in order to assess error levels in the data. For each target, measurements were made at a number of current injection frequencies in order to assess any spectral characteristics and understand possible limitations in the field. Details of the data acquisition system can be found in [7].

4.2 Inversion results

Figure 2 shows example results for the 'copper tube' target. Results are shown for a 4Hz input frequency in terms of magnitude and phase produced by the inversion algorithm above. Also shown is the location of the target.

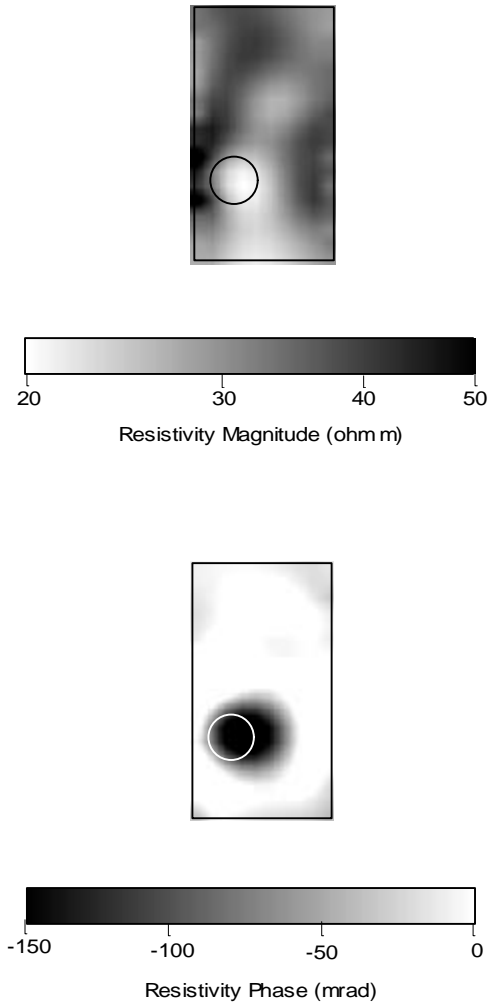


Figure 2: Example results of the complex resistivity inversion using the 'copper target'

The results demonstrate clearly that for this particular target, the inversion is able to satisfactorily identify both a variation in real and imaginary components of the resistivity structure. In this case it is recognised that the phase anomaly is extremely large, nevertheless this serves as a useful demonstration of the algorithm under development.

For comparison figure 3 shows results at 4Hz for the PVC target. In this case, as expected, the resistive anomaly is clearly shown in the magnitude image. The phase image also reveals minimal reactive component in the data (note the change in scale, in comparison to figure 2). Only minor variation of the imaginary component of

resistivity is seen in close proximity to the electrodes, probably a result of polarisation at the electrodes.

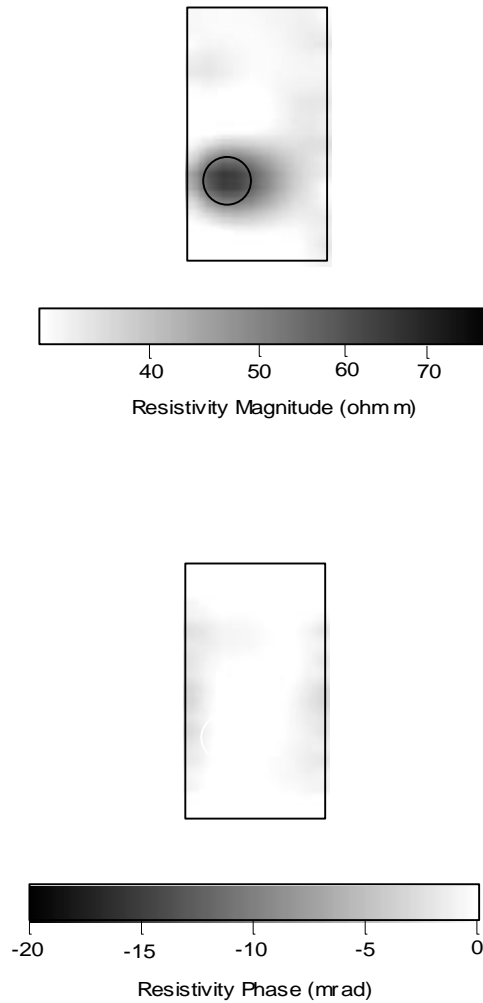


Figure 3: Example results of the complex resistivity inversion using the 'PVC target'

4.3 Spectral properties

Complex resistivity may provide additional information about the composition of the target of interest, however, the method, when used in a spectral manner may also yield additional characteristics about the body under investigation. Figure 4 shows results of the complex inversion for both PVC and copper targets over a range of input frequencies (0.0625Hz to 64Hz).

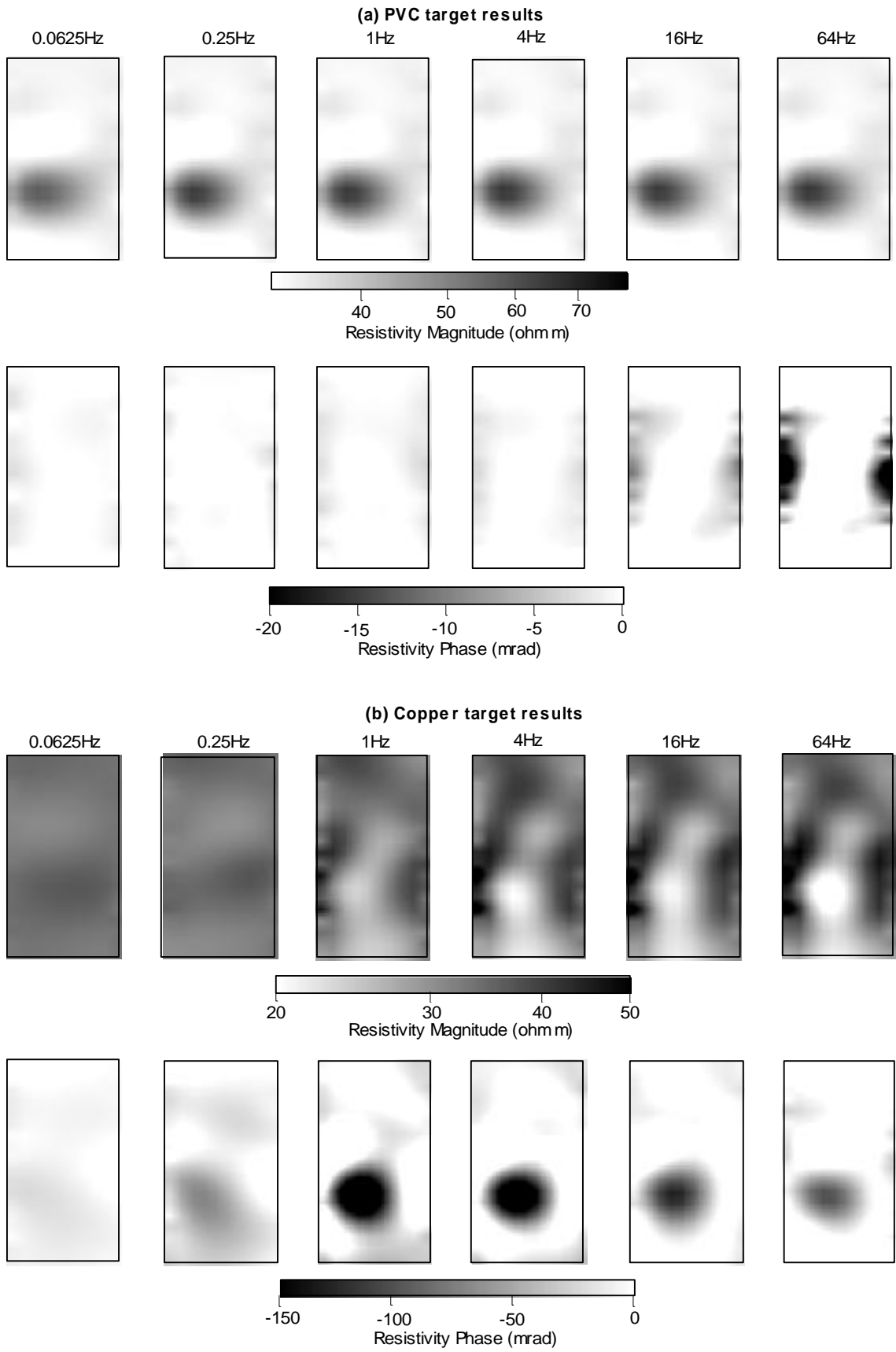


Figure 4: Results from inversion of (a) PVC and (b) copper data

The PVC target results reveal a clear resistive anomaly throughout all applied frequencies, with little variation in the magnitude. The phase images show very low, typically less than 5 mrad, values except at the two highest frequencies. These are clearly due to errors in components of the experimental procedure, caused by electrode effects, instrumentation errors, inappropriate assessment and/or treatment of data errors, modelling errors, and electromagnetic coupling effects. As the phase signals of the target here are so low (theoretically zero) the images act as a useful guide for the combined effect of these errors.

The copper target results in figure 4 show a contrasting result. Here the magnitude shows some change over applied frequency, more important perhaps is the phase response with frequency. Here the target signals appear to dominate any erroneous phase in the data and consequently the images show a clear phase feature at the location of the copper tube target, even at the 64Hz frequency.

To investigate further the change in complex resistivity with frequency it is necessary to examine individual parameter values. Figure 5 shows the location of a parameter selected for this purpose.

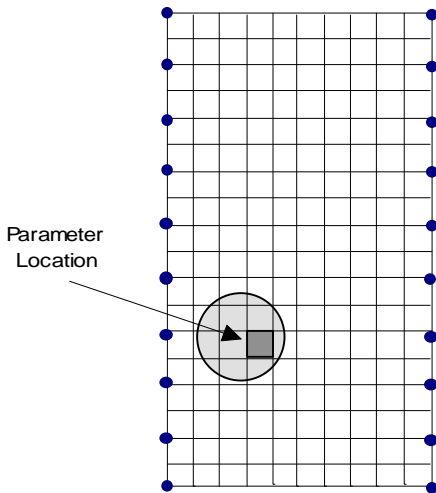


Figure 5: Location of parameter value used for illustration of spectral properties of copper target results.

In figure 6 the variation in complex resistivity is shown for the parameter representing the actual target (identified in figure 5). The shape follows the classical Cole-Cole dispersion, given by:

$$r(\omega) = r_0 \left[1 - m \left(1 - \frac{1}{1 + (i\omega t)^c} \right) \right] \quad (4)$$

where r_0 is the DC resistivity, m is the chargeability, $\omega = 2\pi f$, t is a time constant (or relaxation time) and c describes the frequency dependence. The Cole-Cole model has been used widely in mineral exploration (see for example [8]) to characterise properties of rocks in terms of their mineral composition. Different grain size distributions and mineral types exhibit different types of relaxation spectra and thus frequency characteristics such as in figure 6 can yield useful information about the subsurface.

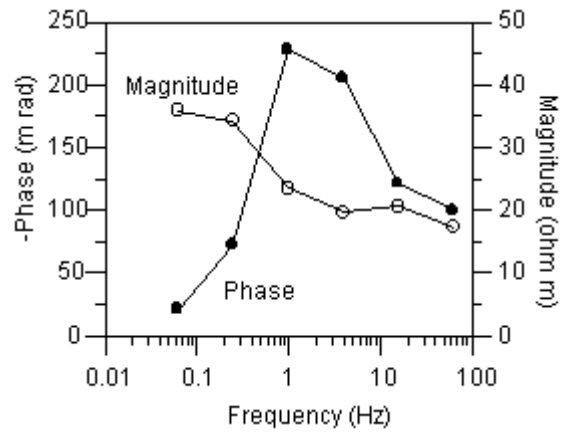


Figure 6: Variation in complex resistivity with frequency for parameter in figure 5 for copper target

5. CONCLUSIONS

With new tomographic inversion methods, such as those presented here, it is, in theory, possible to now apply complex resistivity imaging to arbitrary electrode arrangements. These may be in a borehole to borehole arrangement or geometry more typical of biomedical or process tomography studies.

We expect tomographic methods to play a major role in these new investigations. What remains to be seen is the resolution and accuracy required in data acquisition in order to be able to satisfactorily distinguish material and pore fluid changes in the subsurface environment. Our demonstration here has focussed on targets with significantly different characteristics. For practical application in a wider field we are likely to be limited to more subtle contrasts.

ACKNOWLEDGEMENTS

Continued comments and advice from Andreas Kemna is very much appreciated.

REFERENCES

- [1] Olhoeft, G. R., 1986, Direct detection of hydrocarbon and organic chemicals with ground-penetrating radar and complex resistivity: Proc. NWWA/API Conf. On Petroleum Hydrocarbons and Organic Chemicals in Ground Water - Prevention, Detection, and Restoration, 284-305.
- [2] Börner, F., Gruhne, M., and Schön, J., 1993, Contamination indications derived from electrical properties in the low frequency range: Geophys. Prosp., 41, 83-98.
- [3] Vanhala, H., 1997, Mapping oil-contaminated sand and till with the spectral induced polarization (SIP) method: Geophys. Prosp., 45, 303-326.
- [4] LaBrecque, D. J., Miletto, M., Daily, W., Ramirez, A., and Owen, E., 1996, The effects of noise on Occam's inversion of resistivity tomography data: Geophysics, 61, 538-548.
- [5] deGroot-Hedlin, C., and Constable, S., 1990, Occam's inversion to generate smooth, two-dimensional models from magnetotelluric data: Geophysics, 55, 1613-1624.
- [6] Morita, N., Kumagai, N., and Mautz, J. R., 1990, Integral equation methods for electromagnetics: Artech House, Boston and London, 315-320.
- [7] Daily, W., Ramirez, A., and Zonge, K., 1996, A unique data acquisition system for electrical resistance tomography: in Proc. Symp. on the Application of Geophysics to Engineering and Environmental Problems: EEGS, Keystone, Colorado, 28 April - 2nd May, 743-751.
- [8] Pelton, W.H., Ward, S.H., Hallof, P.G., Sill, W.R. and Nelson, P.H., 1978. Mineral discrimination and removal of inductive coupling with multifrequency IP. Geophysics, 43. 588-609.